# New insight into the local structure of hydrous ferric arsenate using full-potential multiple scattering analysis, density functional theory calculations, and vibrational spectroscopy

Shaofeng Wang[1], Xu Ma[1], Guoqing Zhang[1], Yongfeng Jia[2,*], Keisuke Hatada[3]

1. Key Laboratory of Pollution Ecology and Environmental Engineering, Institute of Applied Ecology, Chinese Academy of Sciences, Shenyang, 110016, China

2. Institute of Environmental Protection, Shenyang University of Chemical Technology, Shenyang, 110142, China

3. Département Matériaux Nanosciences, Institut de Physique de Rennes, UMR UR1-CNRS 6251, Université de Rennes 1, 35042 Rennes Cedex, France

* Corresponding author, Prof. Yonfeng Jia, Email: yongfeng.jia@iae.ac.cn, Tel: +86 (24) 83970503

16 TOC art

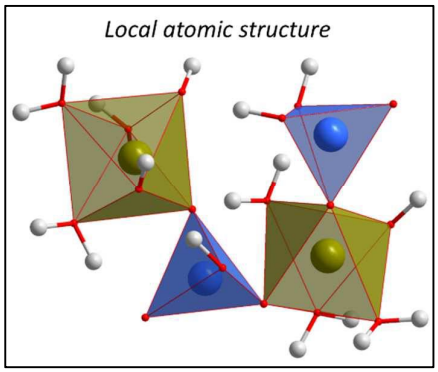


17

18

**ABSTRACT:** Hydrous ferric arsenate (HFA) is an important arsenic-bearing precipitate in the mining-impacted environment and hydrometallurgical tailings. However, there is no agreement on its local atomic structure. The local structure of HFA was re-probed by employing a full-potential multiple scattering (FPMS) analysis, density functional theory (DFT) calculations, and vibrational spectroscopy. The FPMS simulations indicated that the coordination number of the As-Fe and/or Fe-As in HFA was approximately two. The DFT calculations constructed a structure of HFA with the formula of $Fe(HAsO_4)_x(H_2AsO_4)_{1-x}(OH)_y \cdot zH_2O$. The presence of protonated arsenate in HFA was also evidenced by vibrational spectroscopy. The As and Fe *K*-edge XANES spectra of HFA were accurately reproduced by FPMS simulations using the chain structure, which was also a reasonable model for EXAFS fitting. The FPMS refinements indicated that the interatomic Fe-Fe distance was approximately 5.2 Å, consistent with that obtained by Mikutta et al. (*ES&T*, 2013) using wavelet analysis. All of the results suggested that HFA was more likely to occur as a chain with $AsO_4$ tetrahedra and $FeO_6$ octahedra connecting alternately in an isolated bidentate-type fashion. This finding is of significance for understanding the fate of arsenic and the formation of ferric arsenate minerals in an acidic environment.

## INTRODUCTION

Hydrous ferric arsenate (HFA) is one of the important secondary arsenic precipitates in the mining-impacted environment and hydrometallurgical tailings,[1-5] such as acidic mining drainage [6] and gold[7] and uranium mine tailings.[4, 8, 9] In the Fe-As coprecipitation process, a widely employed method for the removal and fixation of arsenic from hydrometallurgical raffinates, HFA precipitates as a major arsenic-bearing phase at acidic pH values.[10] The adsorbed arsenate on ferrihydrite was also observed to transform into HFA at pH values of 3-5.[2, 3] HFA is thermodynamically metastable and can convert to scorodite during prolonged aging at ambient temperature[5] or elevated temperatures.[3, 11] Therefore, precipitation of HFA followed by heat treatment was also employed for the synthesis of scorodite,[1, 4, 12-14] and this could provide an alternative method for the removal and fixation of arsenic in hydrometallurgical solutions with conventional autoclave[15] and ambient pressure scorodite precipitation technology.[16-18]

The local atomic structure of HFA controls its environmental behaviors and recrystallization process. Although various techniques, including X-ray diffraction (XRD),[2, 3] Fourier transform infrared (FTIR) spectroscopy,[3] total X-ray scattering (TXS),[19] synchrotron-based extended X-ray absorption fine structure spectroscopy (EXAFS),[6, 8, 20-22] and wavelet analysis,[22] have been utilized to characterize the structure of HFA, there is still no agreement on its atomic structure.[8, 19-26] Current views regarding the local atomic structure include the framework model,[8, 25] similar to the structure of scorodite, and the chain model,[20, 21, 23, 24] similar to the structures

of butlerite and/or fibroferrite. Both models were proposed mainly based on coordination numbers (CNs) and the interatomic distance of the As-Fe single scattering path derived from shell-fit analysis of As and Fe *K*-edge EXAFS spectra. However, the As-Fe CNs of HFA calculated from EXAFS spectra could vary significantly (1.7 – 4), depending on the fitting strategies and initial model (See Table S1, Supporting Information), thus leading to different conclusions about the local structure of HFA. Chen et al. [8] obtained CNs of 3.2 (As-Fe) and 3.8 (Fe-As) by fitting the EXAFS spectra of HFA and proposed the scorodite-like structure, i.e., arsenate tetrahedra connecting to four $FeO_6$ octahedra and vice versa. In comparison, Paktunc and coworkers obtained CNs of approximately 1.8 for both the As-Fe and Fe-As paths, hence suggesting that the local structure of HFA is better described by the chain model, i.e., single chains of corner-sharing $FeO_6$ octahedra bridged by $AsO_4$ tetrahedra.[20] Mikutta et al. obtained a Fe-Fe interatomic distance of approximately 5.3 Å according to the wavelet transform analysis and the total X-ray scattering results, which is in agreement with the crystallographic data of scorodite and significantly longer than that of the chain model (approximately 3.8 Å) as in butlerite or fibroferrite.[19, 22] They proposed that HFA was composed of isolated $FeO_6$ octahedra bridged by $AsO_4$ tetrahedra.

Compared to the EXAFS spectra, XANES has much stronger oscillation and is more sensitive to the structural details of the absorbing atoms. Based on full multiple scattering (FMS) calculations, XANES features have been widely adopted to probe the interatomic distance and angle of the local structure during the last two

decades.[27-33] Hatada et al. developed the full-potential multiple scattering (FPMS) theory and successfully simulated the XANES spectra of tetrahedrally coordinated cations in $GeCl_4$ or quartz.[34-36] In this study, we used FPMS analysis, in combination with density functional theory (DFT) calculations, EXAFS, and vibrational spectroscopy, to probe the local atomic structure of HFA. This would aid in the understanding of its formation and transformation processes in the environment and hydrometallurgical arsenic removal/fixation operations.

## EXPERIMENTAL

**Synthesis of Hydrous Ferric Arsenate and Scorodite.** HFA was synthesized using sodium arsenate and ferric sulfate solutions according to a previously reported method.[2, 3] In brief, 0.01 mol of As (from $Na_2HAsO_4 \cdot 7H_2O$) and 0.01 mol of Fe (from $Fe_2(SO_4)_3 \cdot 5H_2O$) were added to 500 mL of double distilled water, and the pH of the mixture was adjusted from 1.3 to 1.8 with a 1 M NaOH solution. Then, the mixture was maintained at that pH and room temperature for 3 hours. The resultant solid product was separated by filtration, washed with HCl solution (pH 1.8), and freeze-dried. Scorodite ($FeAsO_4 \cdot 2H_2O$) was also prepared as a reference material by heating a mixture of 0.3 M Fe(III) and 0.3 M As(V) solutions in an autoclave at 175°C for 10 h followed by filtering, rinsing four times with HCl solution (pH 1.8) and freeze drying.[37] Both synthesized materials were characterized using a Rigaku D/Max 2500 X-ray diffractometer with graphite monochromatized Cu$K_{\alpha 1}$ radiation. The XRD patterns of synthetic HFA showed two broad diffraction peaks at 2θ values

of approximately 28° and 58° (Figure S1 in the Supporting Information), which were consistent with previously reported results.[3, 20] After digestion with concentrated hydrochloric acid, the Fe/As molar ratio of HFA was determined to be 1.02±0.01 (n = 3), and the sulfate concentration was lower than 0.01%. The XRD pattern of synthetic scorodite matched well with the standard in the Joint Committee on Powder Diffraction Standards (JSPDS) database (Figure S1).

**X-ray Absorption Spectroscopy (XAS) Measurements.** To collect the XAS spectra, approximately 0.1 g of the synthesized solid was pressed as a disc with a diameter of approximately 1 cm after grinding with an agate mortar and pestle. The As and Fe *K*-edge XAS spectra were obtained on the XAFS beamline at the Beijing Synchrotron Radiation Facility (BSRF). The storage ring was operated at 2.5 GeV and a ring current of 250 mA. A fixed double crystal monochromator with Si(111) crystals was used to monochromatize the white beam. The absolute position of the monochromator was calibrated to 7112 eV for Fe measurements at the first inflection point in the *K*-edge absorption spectrum of Fe foil and at 11919 eV for As measurements by setting the first inflection point in the $L_{III}$-edge absorption spectrum of Au foil. The absorption spectra were collected in the energy range of 6910-7910 eV for the Fe *K*-edge spectra and in the range of 11660-12680 eV for the As *K*-edge spectra in the transmission mode at room temperature. The scan steps were set to 5 eV/step for the pre-edge, 0.5 eV/step for the XANES, and 3-5 eV/step for the EXAFS regions. Each individual sample was scanned three times, and the averaged results are reported.

The pre-processing of spectra was performed by using the Athena program in the Demeter package (version, 0.9.20).[38] The pre-edge of all spectra was fitted with a straight line in the range of 150 – 50 eV before the absorption edge. The post-edge absorption background was subtracted by fitting a cubic polynomial spline to the data in the energy range of 0 – 750 eV after the absorption edge. For Fourier transform, the background cutoff parameter ($R_{bkg}$) was set to 0.9 and 1.0 for As and Fe, respectively.

**EXAFS Analysis.** EXAFS data analysis was performed by fitting the Fourier transformed experimental data with the theoretical amplitude and phase functions calculated by FEFF code. The crystallographic structure of scorodite[39] was used as the FEFF input structure for the EXAFS data of scorodite, whereas the structure of HFA optimized by DFT calculations was used as the model structure of HFA. The least-squares fitting was performed in the *k* ranges of 3–14 $Å^{-1}$ for As and 2–14 $Å^{-1}$ for Fe *K*-edge spectra with Artemis (Demeter package, version 0.9.20) by using a Kaiser−Bessel window function. Based on the fitting results of scorodite, the amplitude reduction factor, $S_0^2$, was set to 1.0 and 0.9 for the As and Fe *K*-edge EXAFS data, respectively.

**XANES Analysis.** The X-ray absorption cross sections from the rising edge energy region to 150 eV for As and 200 eV for Fe *K*-edge XANES spectra after the absorption edge have been analyzed using the recently developed FPMXAN software. For the Fe XANES spectra analysis, the muffin-tin (MT) approximation was used for the shape of the potential.[27, 28, 30] For the As *K*-edge XANES spectra, a

Wigner-Seitz cell was constructed by adding 10 empty spheres around the As atom (Figure S3) based on the FPMS theory.[34-36] The real part of self energy was calculated by using the Hedin-Lunqvist (H-L) potential. Multiple scattering of hydrogen atoms was not considered during the calculations except for the hydrogen atom linked to the central As-O bond. The program used a Monte-Carlo search to alternatively optimize the structure and non-structural parameters (e.g., Fermi energy, energy shift, normalization factor, energy independent broadening, energy dependent broadening, overlapping factor, etc.) until the global minimum of the square residue was achieved. The fitting quality was evaluated using the goodness-of-fit parameter square residue function ($S^2$), which is defined by the following equation:[27, 28]

$$S^2 = n \frac{\sum_{i=1}^{m} w_i \left[ \left( y_i^{th} - y_i^{\exp} \right) \varepsilon_i^{-1} \right]^2}{\sum_{i=1}^{m} w_i} \quad (1)$$

where $n$ is the number of independent parameters, $m$ is the number of data points, $y_i^{th}$ and $y_i^{exp}$ are the theoretical and experimental values of the absorption, respectively, $\varepsilon_i$ is the error in each point of the experimental data set, and $w_i$ is a statistical weight. In this study, $w_i = 1$ was assumed and the square residual function $S^2$ was equaled to the statistical $\chi^2$ function.

**Molecular Orbital Theory Calculations.** The structure of HFA cluster was optimized by performing DFT calculations using ORCA program (V3.0.3) in the gas phase.[40] All energy minimization calculations were carried out without symmetry and atomic constraints. After preliminary tests, hybrid functional B3LYP and def2-TZVP basis set[41] were utilized for geometric optimization, using the resolution

of identity (RI) method. The atom-pairwise dispersion correction with the Becke-Johnson damping scheme (D3BJ)[42] was also applied for all calculations. High-spin $Fe^{3+}$, with each 3d electron occupying one of the five *d*-orbitals, was used for energy minimization. The spin multiplicity of the HFA cluster model (containing two Fe atoms) was set to 11 according to multiplicity = $2S + 1$, where $S$ is the spin of the unpaired electrons.[43] Harmonic vibrational frequencies of the geometrically optimized HFA was also calculated.

**Raman Spectroscopy.** The Raman spectra of synthetic HFA and scorodite were collected on a Raman microscope (Thermo Scientific™ DXR™ xi) equipped with a solid state laser diode operating at 785 nm. A 50X objective lens and 0.8 mW laser were applied. Approximately 50 mg of freeze-dried ground sample was mounted on a glass slide. All samples were measured from 60 to 3300 $cm^{-1}$ in the line focus confocal mode with a detector exposure time of 8 s with the accumulation of 30 spectra. The wavenumber resolution was set at 4 $cm^{-1}$. All of the scans were measured at 10% of the laser output at the microscope exit to avoid radiation damage. Before the measurements, the instrument was calibrated to 520 $cm^{-1}$ by using a standard silicon sample.

**Infrared Spectroscopy.** FTIR spectra were scanned on a Nicolet 6700 Fourier transform infrared spectrometer (Thermo Fisher Scientific, USA). The spectra were collected in a range of 400–4000 $cm^{-1}$ with a spectral resolution of 4 $cm^{-1}$ and 200 co-added scans. Each sample of less than 0.050 mg was mixed with high-purity KBr and then pressed into a disk. Immediately, samples were recorded in the transmission

mode. Peak fitting of infrared spectra was performed using a Lorentzian-Gaussian cross function with the minimum number of peaks. All infrared and Raman spectra were manipulated using the software OMNIC (v 8.2).

## RESULTS AND DISCUSSION

**XANES Analysis.** The normalized As and Fe *K*-edge XANES spectra of scorodite and HFA are compared in Figure 1a and 1b. The figures show obvious differences at 11876-11888 eV and 11934-11980 eV for As as well as 7126-7135 eV and 7183-7300 eV for Fe *K*-edge XANES spectra, indicating that the structure of HFA is different from that of scorodite. The As and Fe *K*-edge XANES spectra of scorodite were simulated using FPMS calculations (Figure 1c and 1d). The crystallographic data of scorodite with the space group *Pcab* ($a$ = 8.937 Å, $b$ = 10.278 Å, $c$ = 9.996 Å, $\alpha = \beta = \gamma = 90°$) were used as the starting simulation model.[39] The cluster radius used is 8 Å, containing 166 and 150 atoms for the As and Fe *K*-edge XANES spectra simulations, respectively. The results show that the experimental spectra of scorodite were accurately reproduced ($S^2$ = 7.7 for As and $S^2$ = 3.9 for Fe). The small discrepancy between the theoretical and experimental spectra in the first 20 eV from the edge is possibly due to the limited cluster size or an overestimation of the inelastic losses.[28]

The controversy for the local atomic structure of HFA focused on the number and positions of $FeO_6$ octahedra/$AsO_4$ tetrahedra coordinating with the central atoms. Since HFA is the precursor of crystalline scorodite,[3, 5] it could be intuitively assumed

that $FeO_6$ octahedra connect with $AsO_4$ tetrahedra in a similar structure to that of scorodite during the formation of the HFA. Therefore, we extracted the local structure of $AsO_4$ tetrahedra and $FeO_6$ octahedra from the crystallographic data of scorodite as the initial structure to distinguish which structure is proximal to the local structure of HFA (Figure 2). The interatomic distances and angles of the extracted local structure are summarized in Table S2 in the Supporting Information. The theoretical As and Fe *K*-edge XANES spectra of different clusters of $AsO_4$ tetrahedra and $FeO_6$ octahedra were calculated. Only the non-structural parameters were optimized by fixing the atomic positions of each cluster. The comparisons between the theoretical spectra and experimental data are illustrated in Figure 2c and 2d. For As *K*-edge XANES spectra, it can be observed that the calculated spectrum of the configuration A1, representing one $AsO_4$ tetrahedron connecting with four $FeO_6$ octahedra, has significantly stronger oscillations than other clusters in the energy range of 50-80 eV, where it is strongly influenced by the backscattering of Fe atoms. As a result, the $S^2$ of 6.9 for configuration A1 is higher than those derived from clusters A5, A6, and A7 (one $AsO_4$ tetrahedron connects with two $FeO_6$ octahedra), indicating that the A1 configuration is not the best. Consistently, the Fe *K*-edge XANES spectra showed that the configuration F1 (one $FeO_6$ octahedron connects with four $AsO_4$ tetrahedra) did not give the smallest $S^2$ either, implying that the $FeO_6$ octahedron is less likely to connect with 4 $AsO_4$ tetrahedra in a manner similar to that of scorodite. These results suggested that in HFA, one $AsO_4$ tetrahedron/$FeO_6$ octahedron is more likely to connect with two $FeO_6$

octahedra/$AsO_4$ tetrahedra as a chain rather than a scorodite-like structure.

Furthermore, the XANES spectra are also very sensitive to the Fe-O-As angle between $AsO_4$ tetrahedra and $FeO_6$ octahedra.[28, 44] It can be clearly observed from Figures 2c and 2d that the clusters of $AsO_4$ tetrahedra and $FeO_6$ octahedra with different angles showed different goodness-of-fit parameters, $S^2$. Simulations for three Fe (As) second-shell neighbors of As (Fe) were also performed (Figure S4, Supporting Information). The clusters A5 ($S^2$ = 4.6) and F5 ($S^2$ = 1.0) showed the best simulation for the experimental data, indicating that the structure of HFA may correspond to a chain structure with $AsO_4$ tetrahedra connecting to two $FeO_6$ octahedra at vertices through atoms O2 and O3.

**Density Functional Theory Calculation Results.** Given that the average crystallite size of the initial HFA precipitates was estimated to be approximately 0.8 – 1 nm,[19, 20] the initial structure of HFA cluster with 2 $AsO_4$ tetrahedra and 2 $FeO_6$ octahedra connecting at vertices through atoms O2 and O3 was constructed based on the XANES simulation results above. Some hydrogen atoms were added to Fe-O bond to achieve charge balance. After energy minimization, the optimized HFA structure showed that the $AsO_4$ groups occurred as $HAsO_4^{2-}$ group in the middle of the chain and as $H_2AsO_4^-$ at the end of the chain, suggesting a structural formula of $Fe(HAsO_4)_x(H_2AsO_4)_{1-x}(OH)_y \cdot zH_2O$ (hydrous basic ferric hydrogen arsenate, $0.5<x<1$, $y=2-x$) (Figure 3). This result is reasonable because arsenate prefers to exist as protonated arsenate species (i.e., $H_3AsO_4^0$ and $H_2AsO_4^-$) at acidic pH values (pH 1 – 2) where HFA precipitates. The calculated bond lengths of As-O in optimized HFA

cluster were in the range of 1.62–1.77 Å, with an average of 1.69±0.048 Å. The calculated bond lengths of Fe-O were in the range of 1.85–2.15 Å, with a mean value of 2.01±0.11 Å. The interatomic distance of Fe-Fe was approximately 5.25 Å.

Based on the DFT-optimized structure, the As and Fe *K*-edge XANES spectra of HFA were simulated. It can be observed that the XANES spectra were accurately simulated with $S^2 = 3.3$ for As and $S^2 = 1.3$ for Fe (Figure 4a & 4b), indicating that our chain model is reasonable. Then, the interatomic distances between absorbing atoms and back scattering atoms were optimized for As and Fe *K*-edge XANES spectra to achieve the best of the As-O and Fe-O bonds. Excellent agreement between the theoretical data and experimental spectra was achieved for both the As ($S^2 = 3.2$) and Fe ($S^2 = 0.19$) *K*-edge XANES spectra (Figure 4c and 4d). The structural optimization of the XANES spectra gave As-O bond lengths of 1.61 – 1.74 Å, with an average of 1.67±0.046 Å, which was comparable to the values derived from DFT calculations and EXAFS data (Table 1). The refined Fe-O bond lengths ranged from 1.84 to 2.15 Å, with an average of 1.99±0.11 Å, which was slightly shorter than those from DFT calculations and EXAFS data (Table 1). In addition, the FPMS optimization of the Fe *K*-edge XANES spectra gave an average interatomic Fe-Fe distance of 5.22 Å, which is highly consistent with the DFT result (~ 5.25 Å) and the value of approximately 5.3 Å derived from the wavelet analysis reported by Mikutta et al.[7] These results further implied that our chain structure was reasonable for HFA.

Paktunc and coworkers argued that the local structure of HFA is similar to those

of the ferric sulfates butlerite ($FeSO_4(OH)\cdot 2H_2O$) and fibroferrite ($FeSO_4(OH)\cdot 5H_2O$), which consist of corner-sharing $FeO_6$ octahedra single chains bridged by $SO_4$ tetrahedra.[20, 23, 24] To verify this hypothesis, the structures of butlerite and fibroferrite were modified by replacing the S atoms with As atoms, and were optimized using DFT calculations. The optimized structures are shown in Figure S5 in the Supporting Information. The Fe-Fe interatomic distances in optimized butlerite-like and fibroferrite-like structures were 3.78 Å and 3.65 Å on average, respectively, which were significantly shorter than those from the DFT calculations (5.25 Å), the FPMS refinement (5.22 Å) and the wavelet analysis of the Fe *K*-edge EXAFS data (~5.3 Å).[21] Furthermore, the theoretical As and Fe *K*-edge XANES spectra calculated using FPMS theory based on the optimized structures were compared with the experimental data. Significant differences were observed for both As ($S^2 = 10.3$ for butlerite and $S^2 = 7.9$ for fibroferrite) and Fe ($S^2 = 2.2$ for butlerite and $S^2 = 4.2$ for fibroferrite) (see Figure S6 in the Supporting Information). These results indicated that the chain structure of corner sharing $FeO_6$ was unlikely to be a reasonable model to describe the local atomic structure of HFA.

**EXAFS Analysis.** Fourier transforms of As and Fe *K*-edge EXAFS data of synthetic scorodite and HFA are compared in Figure 5. Consistent with previous reports,[8, 22] the magnitudes of the Fourier transform peaks of HFA at $R + \Delta R \sim 2.9$ Å for the As *K*-edge EXAFS spectra and $R + \Delta R \sim 3.0$ Å for the Fe *K*-edge EXAFS spectra, with both attributed to the As-Fe oscillations, are less than half of those of crystalline scorodite. This was thought to be the result of lower CNs of the nearest

Fe/As atoms around the absorbers or large variation in the Fe-As interatomic distance.[22] The As and Fe *K*-edge EXAFS spectra were fitted by using the DFT optimized cluster structure of HFA as a model structure. The detailed least-square fitting results are summarized in Table S3 in the Supporting Information. The satisfactory goodness-of-fit parameters, *R*-factor (0.008 for As and 0.006 for Fe) and reduced $\chi^2$ (110 for As and 28 for Fe), were obtained for both the As and Fe *K*-edge EXAFS data. As described above, comparisons in Table 1 show that the mean interatomic distances of As-O (1.68 Å, CN = 4), Fe-O (2.00 Å, CN = 6), and As-Fe (3.30 Å, CN = 1.5) are comparable to those derived from DFT calculations and FPMS analysis. These data further demonstrated that the chain structure of HFA proposed in this study is reliable.

**Infrared and Raman Spectroscopy.** Figure 6, Figure S7 and Figure S8 illustrate the infrared and Raman spectra of synthetic HFA and scorodite. The assignments of infrared and Raman bands for scorodite and HFA are listed in Table S4 in the Supporting Information.

The deconvoluted bands of infrared (400 – 1200 $cm^{-1}$) and Raman spectra (60 – 1200 $cm^{-1}$) for HFA are consistent (Figure 6). Due to the poorly crystalline nature, the bands on infrared and Raman spectra of HFA are poorly resolved and may represent composite of different vibrations. The shape and positions of the infrared and Raman bands of HFA are different from those of scorodite indicating that the protonation and/or metal complexation of $AsO_4$ tetrahedra in HFA was different from in scorodite.[41, 43, 45] According to the DFT calculated frequencies and previously

reported infrared and Raman spectra of (hydrogen) arsenate group-bearing solids (Figure S9 and Table S4),[45-51] the intense HFA infrared bands at 827 and the Raman bands at 825 may be attributed to the composite of $v_1$ $AsO_3$ symmetric stretching vibration from $HAsO_4^{2-}$ groups and As-OFe stretching vibrations from $H_2AsO_4^-$ groups.[52] The infrared band at 877 $cm^{-1}$ and Raman band at 889 $cm^{-1}$ could be assigned to the $v_3$ $AsO_3$ antisymmetric stretching vibration from $HAsO_4^{2-}$ groups.[47-49] The infrared band at 951 $cm^{-1}$ is possibly attributed to the $v_3$ $AsO_2$ antisymmetric stretching vibration from $H_2AsO_4^-$ group.[51] The Raman bands at 985 $cm^{-1}$ and weak infrared bands at 1048 and 1108 $cm^{-1}$ may be attributed to the $v_1$ symmetric stretching vibration of $SO_4^{2-}$ impurity.[50, 53] The shoulder bands at 748 $cm^{-1}$ (infrared) and 766 $cm^{-1}$ (Raman), locating in the range of As-OH stretching vibrations (707–772 $cm^{-1}$)[45-48, 50], could be assigned to the composite of As-OH stretching vibrations from $H_2AsO_4^-$ groups and As-OFe stretching vibrations from $HAsO_4^{2-}$ groups. Other observed bands were assigned to the following vibrations: 213 and 271 $cm^{-1}$ in the Raman spectrum to the lattice vibrations; 424 $cm^{-1}$ of the infrared spectrum and 360 and 412 $cm^{-1}$ in the Raman spectrum to the composite of the $v_2$ $HAsO_4^{2-}/H_2AsO_4^-$ symmetric bending; 481 $cm^{-1}$ of the infrared spectrum and 469 $cm^{-1}$ of the Raman spectrum to the $v_4$ $HAsO_4^{2-}/H_2AsO_4^-$ antisymmetric bending; and a broad weak band at 605 $cm^{-1}$ in the infrared spectrum to the $FeOH/OH_2$ stretching vibrations and/or As-OH stretching vibrations from $H_2AsO_4^-$ groups.[46-49, 51] Although these results cannot provide clear information on the $HAsO_4^{2-}/H_2AsO_4^-$ ratios, the presence of protonated $AsO_4$ groups in HFA is evidenced by the As-OH stretching vibration

345 bands.

346

347 **IMPLICATIONS**

348 The local atomic structure of synthetic HFA was re-probed using FPMS
349 calculations, EXAFS spectra, DFT calculations, and vibrational spectroscopy. The
350 short chain structure with $HAsO_4^{2-}$/$H_2AsO_4^-$ tetrahedra and $FeO_6$ octahedra alternately
351 connected at vertices was found to be a reasonable model for HFA. The butlerite
352 and/or fibroferrite-like chain modes proposed by Paktunc et al.[20] and the
353 scorodite-like model proposed by Chen et al.[8] are unlikely reasonable. The structural
354 information obtained in this study is of significance for understanding the fate of
355 arsenic in some surface environments because HFA is a widely occurring precipitate
356 in the mining-impacted environment and engineered systems, e.g., acid mine drainage
357 and hydrometallurgical tailings,[2, 3, 54] and is the precursor of various crystalline ferric
358 arsenate compounds (i.e., $FeAsO_4 \cdot 2H_2O$, $FeH_3(AsO_4)_2 \cdot 10H_2O$, and
359 $Fe(H_2AsO_4)_3 \cdot 5.5H_2O$) at 25°C depending on the pH values.[5] It would be easier for the
360 HFA with our model structure to convert to ferric hydrogen arsenate minerals
361 ($FeH_3(AsO_4)_2 \cdot 10H_2O$, and $Fe(H_2AsO_4)_3 \cdot 5.5H_2O$) than the scorodite model which
362 consists of isolated $AsO_4$ tetrahedron connecting to four $FeO_6$ octahedra, and vice
363 versa. It is also easier for the structure we proposed to transform to scorodite than the
364 butlerite and/or fibroferrite-like structure consisting of single chains of corner-sharing
365 $FeO_6$ octahedra bridged by $AsO_4$ tetrahedra which needs breakage of Fe-O-Fe bonds.
366 The findings of the present work could also explain the reason why HFA showed

significantly higher solubility than scorodite[4] which needs to break four covalent bonds to dissolve.

## ASSOCIATED CONTENT

**Supporting Information.** Additional information contains the XRD patterns, the SEM images, the Wigner-Seitz cell, the DFT-optimized butlerite-like and fibroferrite-like chain structures and their the theoretical As and Fe K-edge XANES spectra, infrared and Raman spectra, previously reported As-Fe CNs, interatomic distance and bond angle in the local scorodite structure, the EXAFS fitting parameters, and frequency assignments.

## AUTHOR INFROMATION

**Corresponding Author**

*Telephone: Tel: +86 (24) 83970503. Email: yongfeng.jia@iae.ac.cn.

**Present Address**

No.72, Wenhua Road, Shenyang, China, 110016.

**Notes**

The authors declare no competing financial interest.

## ACKNOWLEDGEMENTS

We thank the staff of the XAFS beamline at the Beijing Synchrotron Radiation Facility for their help with the As and Fe *K*-edge XAS spectral measurements. This

work was financially supported by the National Natural Science Foundation of China (No. 41530643), the Strategic Priority Research Program of the Chinese Academy of Sciences (No. XDB14020203) and the National Natural Science Foundation of China (Nos. 41303088 and 41473111). We also gratefully acknowledge the European FP7 MSNano network under Grant Agreement (No. PIRSES-GA-2012-317554), COST Action MP1306 EUSpec, and the Marie Curie Intra-European Fellowship MS-BEEM (No. PIEF-GA-2013-625388).

## REFERENCES

(1) Krause, E.; Ettel, V. A., Solubilities and Stabilities of Ferric Arsenate Compounds. *Hydrometallurgy* **1989,** *22* (3), 311-337.

(2) Jia, Y. F.; Xu, L. Y.; Fang, Z.; Demopoulos, G. P., Observation of surface precipitation of arsenate on ferrihydrite. *Environ Sci Technol* **2006,** *40* (10), 3248-3253.

(3) Jia, Y. F.; Xu, L. Y.; Wang, X.; Demopoulos, G. P., Infrared spectroscopic and X-ray diffraction characterization of the nature of adsorbed arsenate on ferrihydrite. *Geochim Cosmochim Ac* **2007,** *71* (7), 1643-1654.

(4) Langmuir, D.; Mahoney, J.; Rowson, J., Solubility products of amorphous ferric arsenate and crystalline scorodite ($FeAsO_4 \cdot 2H_2O$) and their application to arsenic behavior in buried mine tailings. *Geochim Cosmochim Ac* **2006,** *70* (12), 2942-2956.

(5) Nishimura, T.; Robins, R. G., Crystalline phases in the system

411 Fe(III)-As(V)-$H_2O$ at 25C. In *Second International Symposium on Iron control and*
412 *disposal in Hydrometallurgy*, Dutrizac, J.; Harris, G. B., Eds. Canadian Institute of
413 Mining Metallurgy and Petrolenm: Ottawa Canada, 1996; p 521.
414 (6) Maillot, F.; Morin, G.; Juillot, F.; Bruneel, O.; Casiot, C.; Ona-Nguema, G.;
415 Wang, Y. H.; Lebrun, S.; Aubry, E.; Vlaic, G.; Brown, G. E., Structure and reactivity
416 of As(III)- and As(V)-rich schwertmannites and amorphous ferric arsenate sulfate
417 from the Carnoules acid mine drainage, France: Comparison with biotic and abiotic
418 model compounds and implications for As remediation. *Geochim Cosmochim Ac*
419 **2013,** *104*, 310-329.
420 (7) Paktunc, D.; Foster, A.; Heald, S.; Laflamme, G., Speciation and
421 characterization of arsenic in gold ores and cyanidation tailings using X-ray
422 absorption spectroscopy. *Geochim Cosmochim Ac* **2004,** *68* (5), 969-983.
423 (8) Chen, N.; Jiang, D. T.; Cutler, J.; Kotzer, T.; Jia, Y. F.; Demopoulos, G. P.;
424 Rowson, J. W., Structural characterization of poorly-crystalline scorodite,
425 iron(III)-arsenate co-precipitates and uranium mill neutralized raffinate solids using
426 X-ray absorption fine structure spectroscopy. *Geochim Cosmochim Ac* **2009,** *73* (11),
427 3260-3276.
428 (9) Essilfie-Dughan, J.; Hendry, M. J.; Warner, J.; Kotzer, T., Arsenic and iron
429 speciation in uranium mine tailings using X-ray absorption spectroscopy. *Appl*
430 *Geochem* **2012**.
431 (10) Jia, Y. F.; Demopoulos, G. P.; Chen, N.; Cutler, J. N.; Jiang, D. T. In
432 *Preparation, characterization and solubilities of adsorbed and co-precipitated*

433 *iron(III)-arsenate solids*, ***Hydrometallurgy 2003***, PA, Young, C. A.; Alfantazi, A. M.;
434 Anderson, C. G.; Dreisinger, D. B.; Harris, B.; James, A., Eds. TMS: Warrendale: PA,
435 2003; pp 1923-1935.
436 (11) Le Berre, J. F.; Gauvin, R.; Demopoulos, G. P., A study of the crystallization
437 kinetics of scorodite via the transformation of poorly crystalline ferric arsenate in
438 weakly acidic solution. *Colloid Surface A* **2008,** *315* (1-3), 117-129.
439 (12) Dove, P. M.; Rimstidt, J. D., The Solubility and Stability of Scorodite,
440 $FeAsO_4 \cdot 2H_2O$. *Am Mineral* **1985,** *70* (7-8), 838-844.
441 (13) Rochette, E. A.; Li, G. C.; Fendorf, S. E., Stability of arsenate minerals in soil
442 under biotically generated reducing conditions. *Soil Sci Soc Am J* **1998,** *62* (6),
443 1530-1537.
444 (14) Harvey, M. C.; Schreiber, M. E.; Rimstidt, J. D.; Griffith, M. M., Scorodite
445 Dissolution Kinetics: Implications for Arsenic Release. *Environ Sci Technol* **2006,** *40*
446 (21), 6709-6714.
447 (15) Dutrizac, J. E.; Jambor, J. L., The Synthesis of Crystalline Scorodite,
448 Feaso4.2h2o. *Hydrometallurgy* **1988,** *19* (3), 377-384.
449 (16) Filippou, D.; Demopoulos, G. P., Arsenic immobilization by controlled
450 scorodite precipitation. *Jom-Journal of the Minerals Metals & Materials Society*
451 **1997,** *49* (12), 52-55.
452 (17) Demopoulos, G. P.; Droppert, D. J.; Vanweert, G., Precipitation of crystalline
453 scorodite (FeAsO4 · 2H2O) from chloride solutions. *Hydrometallurgy* **1995,** *38* (3),
454 245-261.

(18) Singhania, S.; Wang, Q.; Filippou, D.; Demopoulos, G. P., Temperature and seeding effects on the precipitation of scorodite from sulfate solutions under atmospheric-pressure conditions. *Metall Mater Trans B* **2005,** *36* (3), 327-333.

(19) Mikutta, C.; Schröder, C.; Marc Michel, F., Total X-ray scattering, EXAFS, and Mössbauer spectroscopy analyses of amorphous ferric arsenate and amorphous ferric phosphate. *Geochim Cosmochim Ac* **2014,** *140*, 708-719.

(20) Paktunc, D.; Dutrizac, J.; Gertsman, V., Synthesis and phase transformations involving scorodite, ferric arsenate and arsenical ferrihydrite: Implications for arsenic mobility. *Geochim Cosmochim Ac* **2008,** *72* (11), 2649-2672.

(21) Paktunc, D.; Majzlan, J.; Palatinus, L.; Dutrizac, J.; Klementova, M.; Poirier, G., Characterization of ferric arsenate-sulfate compounds: Implications for arsenic control in refractory gold processing residues. *Am Mineral* **2013,** *98* (4), 554-565.

(22) Mikutta, C.; Mandaliev, P. N.; Kretzschmar, R., New Clues to the Local Atomic Structure of Short-Range Ordered Ferric Arsenate from Extended X-ray Absorption Fine Structure Spectroscopy. *Environ Sci Technol* **2013,** *47* (7), 3122-3131.

(23) Paktunc, D., Comment on "Structural characterization of poorly-crystalline scorodite, iron(III)-arsenate co-precipitates and uranium mill neutralized raffinate solids using X-ray absorption fine structure spectroscopy" by N. Chen, DT Jiang, J. Cutler, T. Kotzer, YF Jia, GP Demopoulos and JW Rowson. *Geochim Cosmochim Ac* **2010,** *74* (15), 4589-4596.

(24) Paktunc, D.; Manceau, A., Comment on "New Clues to the Local Atomic

Structure of Short-Range Ordered Ferric Arsenate from Extended X-ray Absorption Fine Structure Spectroscopy". *Environ Sci Technol* **2013,** *47* (22), 13199-13200.

(25) Jiang, D. T.; Chen, N.; Demopoulos, G. P.; Rowson, J. W., Response to the comment on "Structural characterization of poorly-crystalline scorodite, iron(III)-arsenate co-precipitates and uranium mill neutralized raffinate solids using X-ray absorption fine structure spectroscopy". *Geochim Cosmochim Ac* **2010,** *74* (15), 4597-4602.

(26) Mikutta, C.; Mandaliev, P. N.; Kretzschmar, R., Response to Comment on "New Clues to the Local Atomic Structure of Short-Range Ordered Ferric Arsenate from Extended X-ray Absorption Fine Structure Spectroscopy". *Environ Sci Technol* **2013,** *47* (22), 13201-13202.

(27) Benfatto, M.; Congiu-Castellano, A.; Daniele, A.; Longa, S. D., MXAN: a new software procedure to perform geometrical fitting of experimental XANES spectra. *J Synchrotron Radiat* **2001,** *8*, 267-269.

(28) Benfatto, M.; Della Longa, S., Geometrical fitting of experimental XANES spectra by a full multiple-scattering procedure. *J Synchrotron Radiat* **2001,** *8*, 1087-1094.

(29) Benfatto, M.; Della Longa, S.; Natoli, C. R., The MXAN procedure: a new method for analysing the XANES spectra of metalloproteins to obtain structural quantitative information. *J Synchrotron Radiat* **2003,** *10*, 51-57.

(30) Hayakawa, K.; Hatada, K.; Della Longa, S.; D'Angelo, P.; Benfatto, M., Progresses in the MXAN fitting procedure. *X-Ray Absorption Fine*

*Structure-XAFS13* **2007,** *882*, 111-113.

(31) Monesi, C.; Meneghini, C.; Bardelli, F.; Benfatto, M.; Mobilio, S.; Manju, U.; Sarma, D. D., Local structure in $LaMnO_3$ and $CaMnO_3$ perovskites: A quantitative structural refinement of Mn K-edge XANES data. *Phys Rev B* **2005,** *72* (17), 174104 (pp1-9)

(32) Demchenko, I. N.; Denlinger, J. D.; Chernyshova, M.; Yu, K. M.; Speaks, D. T.; Olalde-Velasco, P.; Hemmers, O.; Walukiewicz, W.; Derkachova, A.; Lawniczak-Jablonska, K., Full multiple scattering analysis of XANES at the Cd L-3 and O K edges in CdO films combined with a soft-x-ray emission investigation. *Phys Rev B* **2010,** *82* (7), 075107 (pp1-11).

(33) Smolentsev, G.; Feiters, M. C.; Soldatov, A. V., Full-potential XANES analysis for 3D local structure investigation of isocyanide Ni complex. *Nucl Instrum Meth A* **2007,** *575* (1-2), 168-171.

(34) Hatada, K.; Hayakawa, K.; Benfatto, M.; Natoli, C. R., Full-potential multiple scattering for x-ray spectroscopies. *Phys Rev B* **2007,** *76* (6), 060102.

(35) Hatada, K.; Hayakawa, K.; Benfatto, M.; Natoli, C. R., Full-potential multiple scattering for core electron spectroscopies. *J Phys-Condens Mat* **2009,** *21* (10), 104206.

(36) Hatada, K.; Hayakawa, K.; Benfatto, M.; Natoli, C. R., Full-potential multiple scattering theory with space-filling cells for bound and continuum states. *J Phys-Condens Mat* **2010,** *22* (18), 185501.

(37) Gomez, M. A.; Assaaoudi, H.; Becze, L.; Cutler, J. N.; Demopoulos, G. P.,

Vibrational spectroscopy study of hydrothermally produced scorodite ($FeAsO_4 \cdot 2H_2O$), ferric arsenate sub-hydrate (FAsH; $FeAsO_4 \cdot 0.75H_2O$) and basic ferric arsenate sulfate (BFAS; $Fe[(AsO_4)_{(1-x)}(SO_4)_{(x)}(OH)_{(x)}] \cdot wH_{(2)}O$). *J Raman Spectrosc* **2010,** *41* (2), 212-221.

(38) Ravel, B.; Newville, M., ATHENA, ARTEMIS, HEPHAESTUS: data analysis for X-ray absorption spectroscopy using IFEFFIT. *J Synchrotron Radiat* **2005,** *12*, 537-541.

(39) Hawthorne, F. C., The hydrogen positions in scorodite. *Acta Crystallographica, Section B (Structural Crystallography and Crystal Chemistry)* **1976,** *B32*, 2891-2.

(40) Neese, F., The ORCA program system. *Wires Comput Mol Sci* **2012,** *2* (1), 73-78.

(41) Xu, X. F.; Truhlar, D. G., Accuracy of Effective Core Potentials and Basis Sets for Density Functional Calculations, Including Relativistic Effects, As Illustrated by Calculations on Arsenic Compounds. *J Chem Theory Comput* **2011,** *7* (9), 2766-2779.

(42) Grimme, S.; Ehrlich, S.; Goerigk, L., Effect of the Damping Function in Dispersion Corrected Density Functional Theory. *J Comput Chem* **2011,** *32* (7), 1456-1465.

(43) Watts, H. D.; Tribe, L.; Kubicki, J. D., Arsenic Adsorption onto Minerals: Connecting Experimental Observations with Density Functional Theory Calculations. *Minerals-Basel* **2014,** *4* (2), 208-240.

(44) Benfatto, M.; Della Longa, S.; D'Angelo, P., The MXAN procedure: a new method of modeling the XANES spectra to obtain structural quantitative information. *X-Ray and Inner-Shell Processes* **2003,** *652*, 362-369.

(45) Myneni, S. C. B.; Traina, S. J.; Waychunas, G. A.; Logan, T. J., Experimental and theoretical vibrational spectroscopic evaluation of arsenate coordination in aqueous solutions, solids, and at mineral-water interfaces. *Geochim Cosmochim Ac* **1998,** *62* (19-20), 3285-3300.

(46) Čejka, J.; Sejkora, J.; Bahfenne, S.; Palmer, S. J.; Plášil, J.; Frost, R. L., Raman spectroscopy of hydrogen-arsenate group ($AsO_3OH$) in solid-state compounds: cobalt mineral phase burgessite $Co_2(H_2O)_4[AsO_3OH]_2 \cdot H_2O$. *J Raman Spectrosc* **2011,** *42* (2), 214-218.

(47) Frost, R. L.; Bahfenne, S.; Cejka, J.; Sejkora, J.; Palmer, S. J.; Skoda, R., Raman microscopy of haidingerite $Ca(AsO_3OH) \cdot H_2O$ and brassite $Mg(AsO_3OH) \cdot 4H_2O$. *J Raman Spectrosc* **2010,** *41* (6), 690-693.

(48) Frost, R. L.; Bahfenne, S.; Čejka, J.; Sejkora, J.; Plášil, J.; Palmer, S. J., Raman spectroscopic study of the hydrogen-arsenate mineral pharmacolite $Ca(AsO_3OH) \cdot 2H_2O$—implications for aquifer and sediment remediation. *J Raman Spectrosc* **2010,** *41* (10), 1348-1352.

(49) Sejkora, J.; Čejka, J.; Frost, R. L.; Bahfenne, S.; Plášil, J.; Keeffe, E. C., Raman spectroscopy of hydrogen-arsenate group ($AsO_3OH$) in solid-state compounds: copper mineral phase geminite $Cu(AsO_3OH) \cdot H_2O$ from different geological environments. *J Raman Spectrosc* **2010,** *41* (9), 1038-1043.

(50) Gomez, M. A.; Becze, L.; Blyth, R. I. R.; Cutler, J. N.; Demopoulos, G. P., Molecular and structural investigation of yukonite (synthetic & natural) and its relation to arseniosiderite. *Geochim Cosmochim Ac* **2010,** *74* (20), 5835-5851.

(51) Chtioui, A.; Benhamada, L.; Jouini, A., Crystal structure, thermal analysis and IR spectroscopic investigation of $(C_6H_9N_2)H_2XO_4$ (X = As, P). *Mater Res Bull* **2005,** *40* (12), 2243-2255.

(52) Yang, J. Q.; Chai, L. Y.; Yue, M. Q.; Li, Q. Z., Complexation of arsenate with ferric ion in aqueous solutions. *Rsc Adv* **2015,** *5* (126), 103936-103942.

(53) Zhang, D.; Yuan, Z.; Wang, S.; Jia, Y.; Demopoulos, G. P., Incorporation of arsenic into gypsum: Relevant to arsenic removal and immobilization process in hydrometallurgical industry. *J Hazard Mater* **2015,** *300*, 272-280.

(54) Murciego, A.; Álvarez-Ayuso, E.; Pellitero, E.; Rodríguez, M. A.; García-Sánchez, A.; Tamayo, A.; Rubio, J.; Rubio, F.; Rubin, J., Study of arsenopyrite weathering products in mine wastes from abandoned tungsten and tin exploitations. *J Hazard Mater* **2011,** *186* (1), 590-601.

581 Table 1. Comparison of interatomic distance (Å) (coordination number) of scorodite
582 and HFA among the results derived from crystallographic data (XRD), total X-ray
583 scattering (TXS), As and Fe *K*-edge EXAFS spectra analysis, DFT calculations, and
584 full-potential multiple scattering analysis (FPMS) of As and Fe *K*-edge XANES
585 spectra

| | XRD[a] | DFT[b] | XANES[b] | EXAFS[b] | TXS[i] |
|---|---|---|---|---|---|
| **Scorodite** | | | | | |
| As-O | 1.67-1.69 (4) | 1.68-1.69 (4) | No data | 1.69[c] (4) | No data |
| As-Fe | 3.33-3.38 (4) | 3.35-3.41 (4) | No data | 3.36[c,d] (4) | No data |
| Fe-O | 1.94-2.11 (6) | 1.94-2.14 (6) | No data | 2.01[d] (6) | No data |
| Fe-Fe | 5.13-5.35 (4) | 5.19-5.45 (4) | No data | No data | No data |
| **HFA** | | | | | |
| As-O | No data | 1.62-1.76 (4) | 1.61-1.74 (4) [e] | 1.68[c] (4) | 1.68 |
| As-Fe | No data | 3.21-3.36 (2) | 3.16-3.38 (1.5)[f] | 3.30[c], 3.33[d] (1.5) | 3.32 |
| Fe-O | No data | 1.85-2.15 (6) | 1.84-2.15 (6) [g] | 2.00[d] (6) | 1.97 |
| Fe-Fe | No data | 5.25 (1) | 5.22[g] (1) | 5.3[h] | No data |

586 [a] The crystallographic data reported by Hawthorne. [b] This study. [c] Data calculated
587 from As *K*-edge EXAFS spectrum. [d] Data calculated from Fe *K*-edge EXAFS
588 spectrum. [e] Data calculated from As *K*-edge XANES spectrum. [f] Averaged value of
589 As-Fe distance from multiple scattering calculation of As and Fe *K*-edge XANES
590 spectrum. [g] Data calculated from Fe *K*-edge XANES spectrum.[h] Data from wavelet
591 analysis of Fe *K*-edge EXAFS data reported by Mikutta et al.[9] [i] Data from total X-ray
592 scattering analysis reported by Mikutta et al.

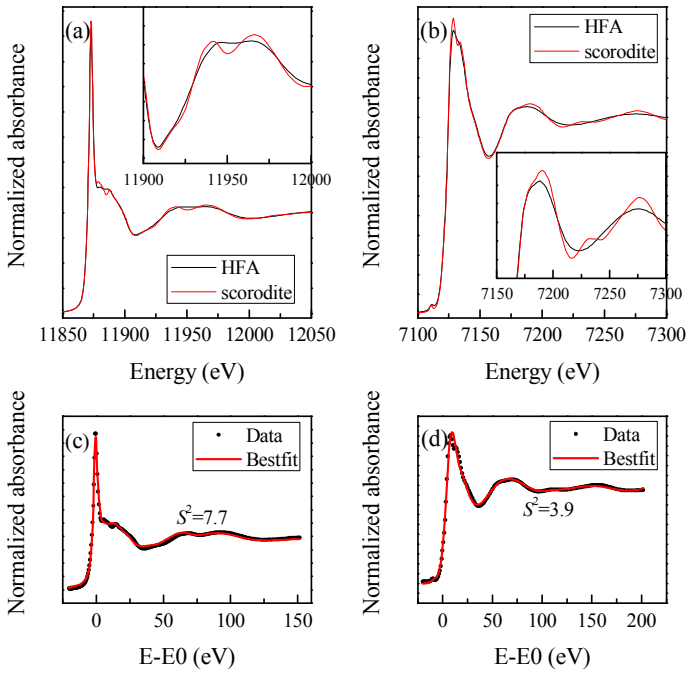


593

594 Figure 1. Arsenic (a) and iron (b) *K*-edge XANES spectra of HFA (black lines) and

595 scorodite (red lines) and the best-fits for As (c) and Fe (d) *K*-edge XANES spectra of

596 scorodite using non-structure optimizations.

597

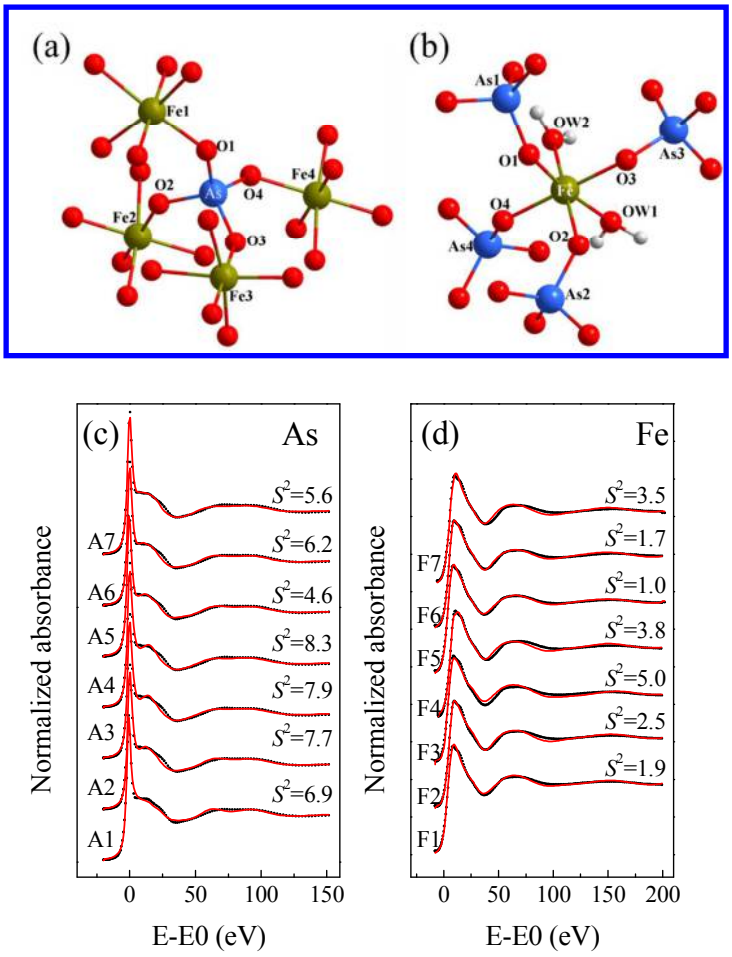


Figure 2. Local atomic structure of scorodite. (a) One arsenate tetrahedron coordinates with four Fe(III)-O octahedra. (b) One Fe(III) octahedron coordinates with four arsenate tetrahedra. Comparison between theoretical arsenic (c) and iron (d) *K*-edge XANES spectra (red solid lines) according to the extracted clusters from scorodite and experimental data (black dotted lines) of HFA. For As *K*-edge spectra, cluster A1-A7 represent As+4Fe, As+Fe1+Fe2, As+Fe1+Fe3, As+Fe1+Fe4, As+Fe2+Fe3, As+Fe2+Fe4, and As+Fe3+Fe4, respectively. For Fe *K*-edge spectra, cluster F1-F7 represent Fe+4As, Fe+As1+As2, Fe+As1+As3, Fe+As1+As4, Fe+As2+As3, Fe+As2+As4, and Fe+As3+As4, respectively.

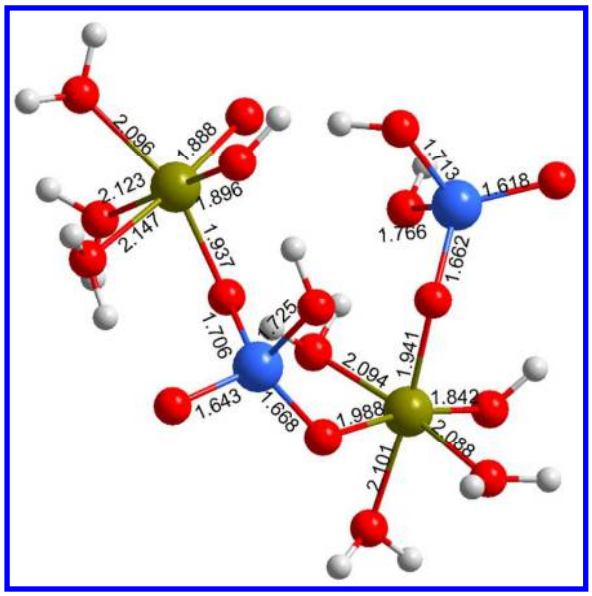


Figure 3. The DFT optimized structure of hydrous ferric arsenate (HFA) cluster.

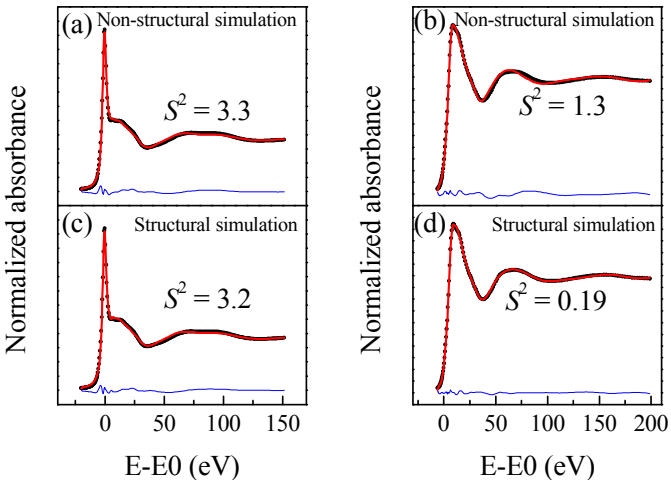


612

613 Figure 4. Comparison of the experimental and theoretical data of non-structural

614 simulation and structural optimized As (left column) and Fe (right column) *K*-edge

615 XANES spectra of HFA. Experimental data, best fits, and residual are shown as black

616 dots, red lines and blue lines, respectively.

617

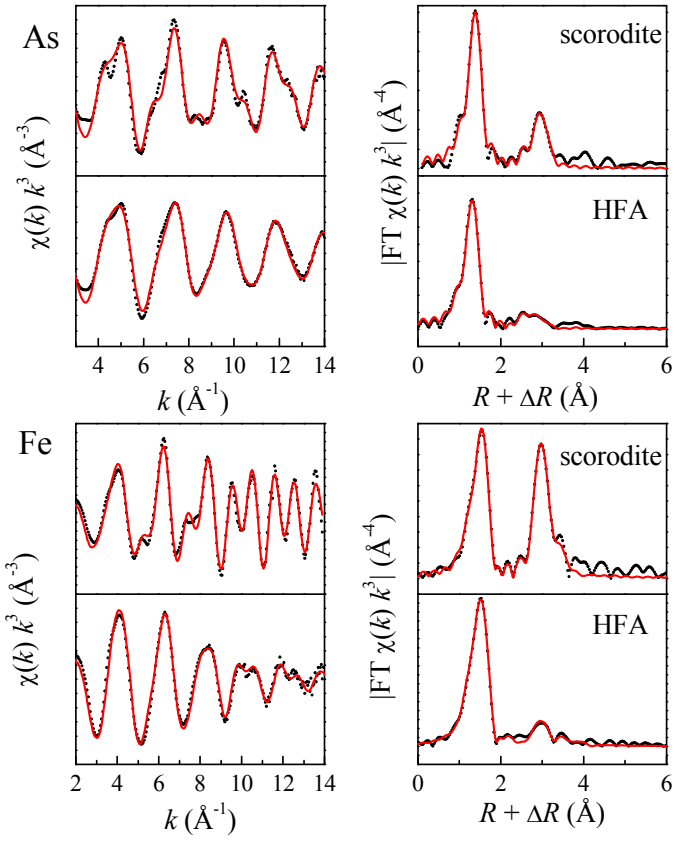


Figure 5. Arsenic and iron *K*-edge $k^3$-weighted EXAFS spectra (left) and the corresponding Fourier transforms (right) of scorodite and HFA based on DFT optimized structure. Experimental data and fits are shown as black dots and red lines, respectively. The fitting results are summarized in Table S5.

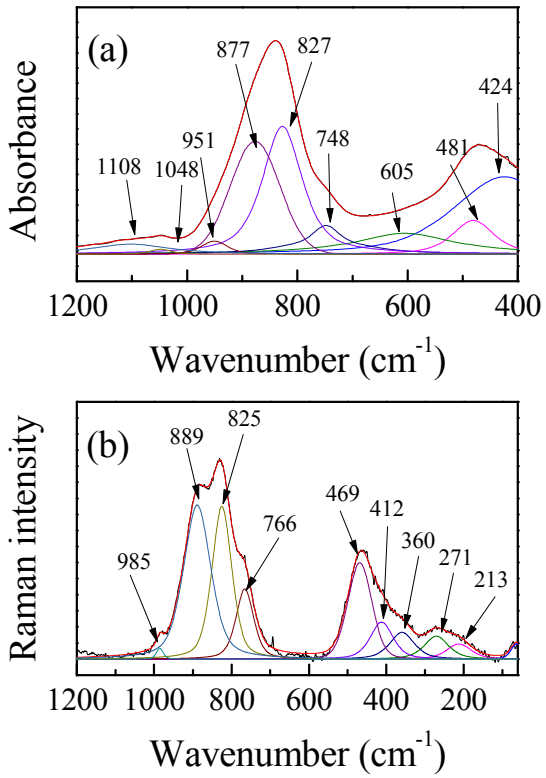


624

625 Figure 6. Deconvoluted infrared (400 – 1200 $cm^{-1}$) (b) and Raman (60 – 1200 $cm^{-1}$) (c)

626 spectra of synthetic scorodite and HFA. Black and red line represent the experimental

627 and fitted spectra, respectively.

628

629 Supporting information to

630 "**New insight into the local structure of hydrous ferric arsenate using**

631 **full-potential multiple scattering analysis, density functional theory calculations,**

632 **and vibrational spectroscopy**"

633

634 Shaofeng Wang[1], Xu Ma[1], Guoqing Zhang[1], Yongfeng Jia[1,2,] *, Keisuke Hatada[3]

635

636 1. Key Laboratory of Pollution Ecology and Environmental Engineering, Institute of

637 Applied Ecology, Chinese Academy of Sciences, Shenyang, 110016, China

638 2. Institute of Environmental Protection, Shenyang University of Chemical

639 Technology, Shenyang, 100049, China

640 3. Département Matériaux Nanosciences, Institut de Physique de Rennes, UMR

641 UR1-CNRS 6251, Université de Rennes 1, 35042 Rennes Cedex, France

642 * Corresponding author, Prof. Yonfeng Jia, Email: yongfeng.jia@iae.ac.cn, Tel: +86

643 24 83970503

644

645 This supporting information contains 9 figures, 4 tables, and references.